



Cite this: *Nanoscale*, 2016, **8**, 17836

Superhalogens as building blocks of two-dimensional organic–inorganic hybrid perovskites for optoelectronics applications†

Qishi Yao,‡^{a,b} Hong Fang,*‡^b Kaiming Deng,^a Erjun Kan*^a and Puru Jena*^b

Organic–inorganic hybrid perovskites, well known for their potential as the next generation solar cells, have found another niche application in optoelectronics. This was demonstrated in a recent experiment (L. Dou, *et al.*, *Science*, 2015, **349**, 1518) on atomically thin $(\text{C}_4\text{H}_9\text{NH}_3)_2\text{PbBr}_4$, where, due to quantum confinement, the bandgap and the exciton binding energy are enhanced over their corresponding values in the three-dimensional bulk phase. Using density functional theory we show that when halogen atoms (e.g. I) are sequentially replaced with superhalogen molecules (e.g. BH_4) the bandgap and exciton binding energy increase monotonically with the superhalogen content with the exciton binding energy of $(\text{C}_4\text{H}_9\text{NH}_3)_2\text{Pb}(\text{BH}_4)_4$ approaching the value in monolayer black phosphorus. Lead-free admixtures $(\text{C}_4\text{H}_9\text{NH}_3)_2\text{Ml}_{4-x}(\text{BH}_4)_x$ ($\text{M} = \text{Sn}$ and Ge ; $x = 0-4$) also show a similar trend. Thus, a combination of quantum confinement and compositional change can be used as an effective strategy to tailor the bandgap and the exciton binding energy of two-dimensional hybrid perovskites, making them promising candidates for optoelectronic applications.

Received 14th July 2016,
Accepted 18th September 2016

DOI: 10.1039/c6nr05573g

www.rsc.org/nanoscale

Introduction

Perovskites with the formula AMX_3 (A and M are metal cations and X is an anion) have been of great interest to scientists since their discovery in 1839. Much of this interest is due to the fact that they can not only be synthesized using a solution-based method but also their composition can be varied widely. Perovskites are multifunctional materials with an impressive range of interesting properties such as superconductivity, giant magnetoresistance, spintronics and catalytic properties. The recent discovery that $\text{CH}_3\text{NH}_3\text{PbI}_3$ can serve as an efficient solar cell material has heightened the interest in the study of organic–inorganic hybrid perovskites.^{1–7} Their potential as the next generation solar cell material is due to a combination of attractive properties such as tunable bandgap,⁸ large optical absorption,² small exciton binding energy,^{9,10} very long carrier diffusion lengths,¹¹ and solution-based synthesis.¹ The meteo-

ric increase in the power conversion efficiency of perovskite-based photo-voltaic devices from 3.8%¹ in 2009 to 20%^{12,13} today makes them the “next big thing” in solar cells.

The use of organic–inorganic perovskites has now gone beyond the solar cells, extending their applications to other important fields such as lasing,¹⁴ field-effect transistors,¹⁵ and photoluminescence devices.^{16–18} The recent breakthrough in synthesizing high-quality atomically thin two-dimensional (2D) hybrid perovskites BA_2MX_4 (BA: butylammonium, $\text{C}_4\text{H}_9\text{NH}_3$; M = Pb; X = I, Br) by the solution-phase growth method⁴ furthered the use of these materials in nanoscale optoelectronic devices such as light-emitting diodes (LED). The above 2D structure consists of corner-sharing $[\text{MX}_6]^{4-}$ octahedra capped by intervening layers of organic cations, as shown in Fig. 1a. The layer of long organic chains is insulating, while the inorganic layer is semiconducting, effectively creating a quantum well (QW) super-lattice. Due to the quantum confinement effect caused by reduced dimensionality, these materials transition from free-carrier to excitonic behavior at room temperature. With a corresponding increase in the exciton binding energy from tens of meV to hundreds of meV and blue to purple light emission, 2D hybrid perovskites are preferred for LED and photoluminescent applications.⁹ The color of the emitted light can be readily tuned by changing the thickness or/and halogen-composition of the 2D materials.

^aDepartment of Applied Physics, and Key Laboratory of Soft Chemistry and Functional Materials (Ministry of Education), Nanjing University of Science and Technology, 210094 Nanjing, China. E-mail: ekan@njust.edu.cn

^bDepartment of Physics, Virginia Commonwealth University, 701 West Grace Street, 23284 VA, USA. E-mail: pjena@vcu.edu, hfangtom@gmail.com

†Electronic supplementary information (ESI) available. See DOI: 10.1039/c6nr05573g

‡These authors contributed equally to this work.

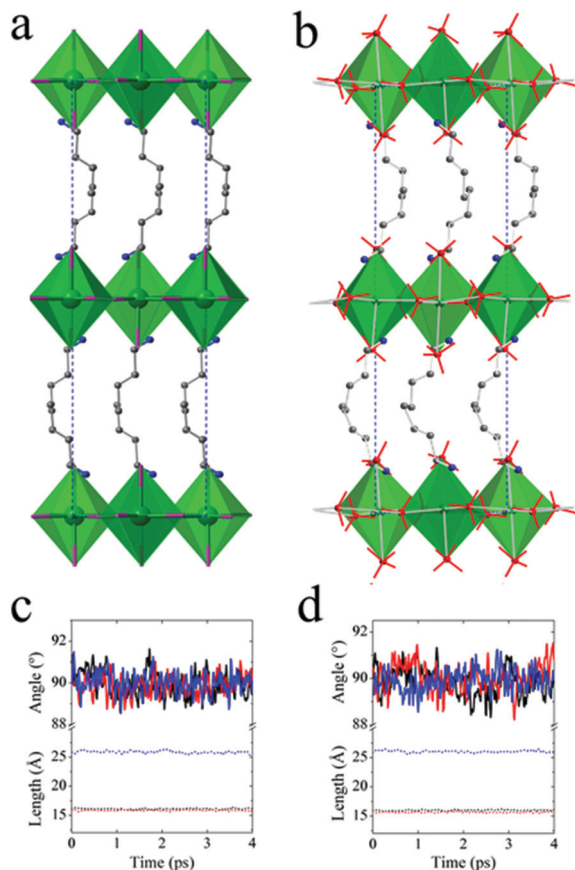


Fig. 1 Crystal structures of (a) BA_2MI_4 and (b) $\text{BA}_2\text{M}(\text{BH}_4)_4$ ($\text{M} = \text{Ge, Sn, Pb}$). The gray and blue balls denote C and N atoms. $[\text{MI}_6]^{4-}$ are in green octahedra. BH_4^- tetrahedra are in red. I and H atoms are omitted for clarity. AIMD-simulated structure parameters of (c) $\text{BA}_2\text{Sn}(\text{BH}_4)_4$ and (d) $\text{BA}_2\text{Ge}(\text{BH}_4)_4$. Lattice angles α , β and γ are in black, red and blue solid lines, respectively. Lattice lengths a , b and c of the $2 \times 2 \times 1$ supercell are in black, red and blue dotted lines, respectively.

In this paper, we propose a new route for tailoring the bandgap and exciton binding energies of 2D hybrid perovskites by sequentially replacing the halogens with molecular units that mimic the chemistry of halogens but are not composed of them. The molecular analogues of halogens are known in the literature as superhalogens¹⁹ whose electron affinities are larger than those of halogens and can be tuned by controlling their composition. There has been a recent experimental study on synthesizing more than 30 new stable perovskites by replacing halogen (Cl, Br, I) with superhalogen BH_4^- .²⁰ Very recently, two of the authors of the current paper showed that 3D hybrid perovskites can be viewed as superalkali halides where the alkali cations and halogens anions are replaced by their molecular equivalent, namely superalkalis, such as $[\text{CH}_3\text{NH}_3]^+$ and $[\text{HC}(\text{NH}_2)_2]^+$, and superhalogens $[\text{MX}_3]^-$ ($\text{X} = \text{halogen}$).²¹ It was also shown that a new class of hydride-based hybrid perovskites with controlled bandgaps can be created by replacing halogen with superhalogen BH_4^- . We note that the ionic radius of BH_4^- is almost identical to that of Br^- in hybrid perovskites.²¹ The bonding ionicity

between the organic cation and the $[\text{M}(\text{BH}_4)_3]^-$ anion is also very similar to that between the same cation and the $[\text{MI}_3]^-$ anion. The hybrid perovskites with BH_4^- show increased bandgap due to the fact that the energy corresponding to the valence band maximum (VBM) of BH_4^- is derived from the hybridized B 2p and H 1s orbitals, which are much lower in energy than the valence shells of halogen atoms. Here, we follow a similar procedure for the 2D hybrid perovskites $\text{BA}_2\text{PbI}_{4-x}\text{Br}_x$ but we use the superhalogen BH_4^- instead of Br^- . Thus created 2D materials are expected to have larger bandgaps and, therefore, larger exciton binding energies than the corresponding halogen-based materials. We also explored lead-free analogues of the 2D materials. In the following, we systematically study 2D $\text{BA}_2\text{MI}_{4-x}(\text{BH}_4)_x$ ($\text{M} = \text{Ge, Sn, Pb}$; $x = 0-4$) for their thermal stability and electronic and excitonic properties.

Computational methods

The geometry and electronic structures of $\text{BA}_2\text{MI}_{4-x}(\text{BH}_4)_x$ ($\text{M} = \text{Ge, Sn, Pb}$; $x = 0-4$) are computed using density functional theory (DFT) with the Perdew–Burke–Ernzerhof (PBE) functional for the generalized gradient approximation (GGA), implemented in the Vienna *ab initio* simulation package (VASP).^{22,23} Structures are relaxed without any symmetry constraint with a cutoff energy of 400 eV. Convergence criteria of energy and force are set to 1×10^{-5} eV and $0.01 \text{ eV } \text{\AA}^{-1}$, respectively. DFT-D2 correction of Grimme^{24,25} is used to account for the van der Waals interactions between organic layers. Reciprocal spaces are represented by the Monkhorst–Pack special k -point scheme²⁶ with $3 \times 3 \times 1$, $5 \times 5 \times 1$, and $7 \times 7 \times 3$ grid meshes for structure optimization, self-consistent field (SCF) and density of states (DOS) calculations, respectively. Band structures are calculated with and without spin–orbit coupling (SOC). Effective masses at the bands' extrema are calculated using the finite difference method with a step size of 0.01 Bohr.²⁷

Ab initio molecular dynamics (AIMD) simulations of hybrid perovskites are performed at the GGA-PBE level of theory embedded in the VASP. A $2 \times 2 \times 1$ supercell containing 880 atoms is used for each simulation. During simulation, both the size and shape of the cells are allowed to change under ambient conditions within the NpT ensemble. The tolerance of the SCF cycle is set to 1×10^{-5} eV. A time step of 1 femtosecond (fs) is chosen. We allow 1 picosecond (ps) for the system to reach thermal equilibrium and then collect atomic trajectory data every 10 fs for 4 ps.

All cluster calculations are carried out using the Gaussian 03 software package.²⁸ The cluster structures are optimized until they reach the energy minimum without imaginary frequencies. HOMO–LUMO gaps are calculated using the second order Møller–Plesset perturbation (MP2)²⁹ theory and the aug-cc-pVDZ basis set. Time-dependent DFT (TD-DFT)³⁰ with the Becke three parameter Lee–Yang–Parr (B3LYP) functional^{31,32} is used to compute the ultraviolet-visible spectrum. The

optical gaps are obtained as the first peak with non-zero oscillator strength in the spectrum.

Results and discussion

Fig. 1b shows the crystal structure of $\text{BA}_2\text{M}(\text{BH}_4)_4$ ($\text{M} = \text{Ge}, \text{Sn}, \text{Pb}$). Similar to the structure of BA_2MX_4 ($\text{X} = \text{halogen}$), each metal ion is octahedrally coordinated to six BH_4^- units. The neighboring octahedra share the vertices and rotate against each other. The lattice parameters of $\text{BA}_2\text{Sn}(\text{BH}_4)_4$ and $\text{BA}_2\text{Ge}(\text{BH}_4)_4$ simulated under ambient conditions by AIMD after the thermal equilibrium is reached (see Fig. S1 in the ESI† for the simulated free energy) are shown in Fig. 1c and d, respectively. These results confirm the thermal stability of these materials in a tetragonal crystal system.

Fig. 2 shows the calculated electronic density of states and band structures of $\text{BA}_2\text{M}(\text{BH}_4)_4$ ($\text{M} = \text{Pb}, \text{Sn}, \text{Ge}$). The partial

DOS for each material shows that the valence band maximum (VBM) is composed of hybridized metal s (Pb: 6s; Sn: 5s; Ge: 4s), B 2p and H 1s orbitals of the BH_4^- superhalogen. The conduction band minimum (CBM) is derived from the metal p orbitals (Pb: 6p; Sn: 5p; Ge: 4p). These results are similar to those in BA_2PbI_4 , where the VBM originates from the Pb 6s and I 5p and CBM is composed of Pb 6p orbitals. Details are also shown for the partial charge density of VBM and CBM in ESI Fig. S2.† All the studied materials show a direct bandgap at the Γ point. For $\text{BA}_2\text{Pb}(\text{BH}_4)_4$, the SOC reduces the gap by about 1 eV³³ due to the lowering of the Pb 6p orbital. However, for $\text{BA}_2\text{Sn}(\text{BH}_4)_4$ and $\text{BA}_2\text{Ge}(\text{BH}_4)_4$, the effect of SOC is negligible. Similar behavior of SOC has been observed in their counterparts with I and Br and also in 3D hybrid perovskites. It has been known that, on the one hand, SOC will lower the Pb 6p band, reducing the bandgap, while on the other hand, a strong relativistic effect of Pb will lower its s band, increasing the gap by about the same amount. A PBE gap of

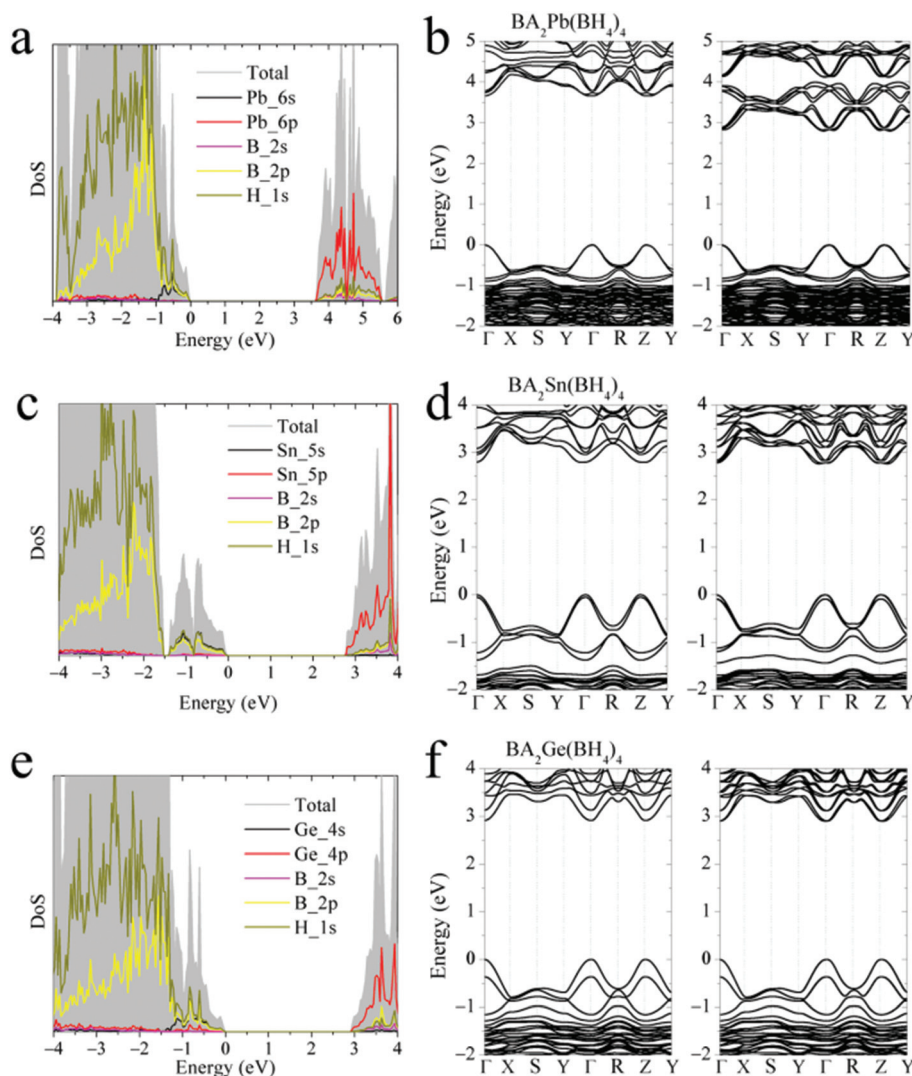


Fig. 2 DOS without SOC of (a) $\text{BA}_2\text{Pb}(\text{BH}_4)_4$, (c) $\text{BA}_2\text{Sn}(\text{BH}_4)_4$ and (e) $\text{BA}_2\text{Ge}(\text{BH}_4)_4$. Band structures without (left panel) and with (right panel) SOC of (b) $\text{BA}_2\text{Pb}(\text{BH}_4)_4$, (d) $\text{BA}_2\text{Sn}(\text{BH}_4)_4$ and (f) $\text{BA}_2\text{Ge}(\text{BH}_4)_4$. $\Gamma = (0, 0, 0)$, $X = (0.5, 0, 0)$, $S = (0.5, 0.5, 0)$, $Y = (0, 0.5, 0)$, $R = (0.5, 0.5, 0.5)$, $Z = (0, 0, 0.5)$.

2.09 eV (see ESI Fig. S3†) of BA_2PbI_4 without SOC and relativistic effect is fortuitously in good agreement with the experimental value of 2.24 eV.³⁴ However, the calculated PBE bandgaps of $\text{BA}_2\text{Sn}(\text{BH}_4)_4$ and $\text{BA}_2\text{Ge}(\text{BH}_4)_4$ should be underestimated, as there will no longer be any fortunate cancellation of errors. It should also be noticed that, with SOC correction, CBM of each $\text{BA}_2\text{M}(\text{BH}_4)_4$ ($\text{M} = \text{Pb}, \text{Sn}, \text{Ge}$) shows a splitting against k around the Γ point. This is the so-called Rashba effect, caused by the breaking of centrosymmetry in the crystal structures due to the substitution of halogen by BH_4^- .

Another feature of the band structure is that the dispersions along the $R-\Gamma-Y$ and $R-Z-Y$ directions have mirror symmetry. This is due to the insulating character perpendicular to the inorganic layers, resulting in a flat band along the $\Gamma-Z$ direction. The electrons and holes are well confined in the inorganic layers. Our results show that 2D perovskites are ideal quantum well (QW) structures and BH_4 substitution does not destroy the host materials' QW feature. Effective mass analysis of VBM and CBM further proved our conclusion. Table 1 shows the calculated hole and electron effective masses along the $\Gamma-X$, $\Gamma-Y$ and $\Gamma-Z$ directions in $\text{BA}_2\text{PbI}_{4-x}(\text{BH}_4)_x$ ($x = 0-4$). For $\text{BA}_2\text{SnI}_{4-x}(\text{BH}_4)_x$ and $\text{BA}_2\text{GeI}_{4-x}(\text{BH}_4)_x$ the effective masses are given in ESI Table S1.† As discussed before, the VBM arises from B and H, where SOC is non-effective. However, Pb contributes to the CBM of $\text{BA}_2\text{PbI}_{4-x}(\text{BH}_4)_x$ ($x = 0-4$), and SOC is therefore important for the position and shape of the CBM. Our results show that, compared to the results without SOC, the electron effective mass with SOC tends to be smaller, especially in the case of $\text{BA}_2\text{Pb}(\text{BH}_4)_4$. Also, with SOC, the effective mass of the electron does not increase much from $x = 0$ to $x = 4$. This suggests that the negative impact on the electron effective mass caused by replacing I with BH_4 is limited. Most of the hole and electron effective masses along $\Gamma-X$ and $\Gamma-Y$ are smaller than those of the free electron mass, m_0 . Both hole and electron effective masses along $\Gamma-Z$ are infinite, which shows the QW characteristic of 2D hybrid perovskites.

The bandgap and exciton properties of admixtures $\text{BA}_2\text{MI}_{4-x}(\text{BH}_4)_x$ ($\text{M} = \text{Pb}, \text{Sn}, \text{Ge}$) are also examined. For $\text{BA}_2\text{Pb}(\text{BH}_4)_4$ ($\text{BA} = \text{C}_4\text{H}_9\text{NH}_3$), there are 220 atoms in its unit cell. (There are 4 formula units $\text{BA}_2\text{Pb}(\text{BH}_4)_4$ in one unit cell of the crystal.) Calculations using functionals such as HSE and GW would provide more reliable absolute values of the bandgap of the material, but greatly surpass our computing capacity. On the other hand, according to our previous study on organic-

inorganic hybrid perovskites, we can (at least roughly) estimate the bandgap of the bulk hybrid perovskites by using cluster models.³⁵ The method is that, in admixtures of $\text{AMX}_{4-x}\text{Y}_x$ ($\text{A} = \text{organic cation}; \text{M} = \text{metal}; \text{X} = \text{halogen 1}, \text{Y} = \text{halogen 2}$), the variation of the bandgap from $x = 0$ to $x = 4$ can be estimated from the variation of the fundamental gap of the corresponding cluster model $\text{AMX}_{4-x}\text{Y}_x$. The validity of the method is based on the following. First, the valence band (VB) and the conduction band (CB) of organic-inorganic hybrid perovskites originate from the HOMO and LUMO of the cluster model, respectively. The expansion of the HOMO (LUMO) to VB (CB) can be explained by using a tight-binding model with the molecular cluster as the building block.³⁵ Second, the method has been tested by comparing the estimated bandgaps from the cluster model to the experimental values³⁶⁻⁴¹ in 3D hybrid perovskites, as shown in ESI Table S2.† Third, we consider the studied 2D hybrid perovskites as the special case of 3D hybrid perovskites with a quantum well character along one crystal dimension. Although the lack of experimental bandgaps of admixtures $\text{BA}_2\text{MX}_{4-x}\text{Y}_x$ ($\text{M} = \text{metal}; \text{X} = \text{halogen 1}, \text{Y} = \text{halogen 2}; x = 0-4$) prevents us from testing the method in a more general fashion, the case study in $\text{BA}_2\text{PbI}_{4-x}\text{Br}_x$ where experimental bandgaps are available for $x = 0, 2, 4$ does give us confidence in our prediction, as shown in ESI Fig. S4.† For $x = 2$, the bandgap estimated from the cluster model is 2.68 eV (BA_2PbI_4 experimental bandgap 2.41 eV plus cluster model predicted gap change from $x = 0$ to $x = 2$, 0.27 eV) compared to the experimental value of 2.46 eV, the relative difference being about 9%. For $x = 4$, the value from the cluster model is 3.10 eV (BA_2PbI_4 experimental bandgap 2.41 eV plus cluster model predicted gap change from $x = 0$ to $x = 4$, 0.69 eV) compared with the experimental value of 3.05 eV, the relative difference being about 2%. Although the bandgap values estimated from the cluster model for the admixtures $\text{BA}_2\text{MI}_{4-x}(\text{BH}_4)_x$ ($\text{M} = \text{Pb}, \text{Sn}, \text{Ge}; x = 0-4$) are expected to give the correct trend, more accurate values of the bandgaps obtained from experiments are desirable.

We first calculated the fundamental gaps of the cluster models of the admixtures $\text{BA}_2\text{MI}_{4-x}(\text{BH}_4)_x$ ($\text{M} = \text{Pb}, \text{Sn}, \text{Ge}$). For each case of $\text{M} = \text{Pb}, \text{Sn}$ and Ge , we calculated the fundamental gap variations when $x = 1-4$ against $x = 0$. Then by adding these variations to the experimental bandgap of BA_2MI_4 ($\text{M} = \text{Pb}, \text{Sn}, \text{Ge}$), the bandgaps of $\text{BA}_2\text{MI}_{4-x}(\text{BH}_4)_x$ for $x = 1-4$ were estimated. The cluster model we used for the

Table 1 Effective masses (relative to the electron mass m_0) of $\text{BA}_2\text{PbI}_{4-x}(\text{BH}_4)_x$ for holes and electrons along $\Gamma-X$, $\Gamma-Y$, and $\Gamma-Z$

$\text{BA}_2\text{PbI}_{4-x}(\text{BH}_4)_x$	Hole			Electron				
	$\Gamma-X$	$\Gamma-Y$	$\Gamma-Z$	$\Gamma-X$		$\Gamma-Y$		$\Gamma-Z$
				Non-SOC	SOC	Non-SOC	SOC	
x								
0	0.27	0.27	∞	0.27	0.28	0.18	0.26	∞
1	0.53	0.66	∞	1.15	0.57	0.26	0.34	∞
2	0.47	0.43	∞	0.25	0.19	0.27	0.18	∞
3	0.56	0.68	∞	0.34	0.56	0.42	0.53	∞
4	0.46	0.45	∞	0.69	0.61	5.48	0.83	∞

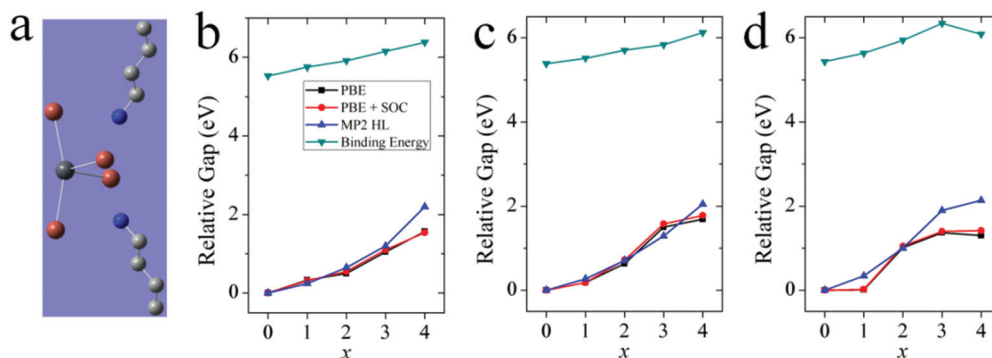


Fig. 3 (a) Cluster model of 2D hybrid perovskites. The organic chains of $C_4H_9NH_3$ are in blue and gray stick-and-ball representation. The red balls denote the halogen atoms or BH_4 units surrounding the black metal atom (Pb, Sn or Ge). Calculated relative gaps of $BA_2MI_{4-x}(BH_4)_x$ where M is (b) Pb, (c) Sn and (d) Ge for both bulk materials and cluster models. The exciton binding energies of these admixtures are from the cluster model.

studied admixtures is shown in Fig. 3a. We have normalized all the gaps of BA_2MI_4 (bulk and cluster, $M = Pb, Sn, Ge$) to 0 to highlight the gap change, as shown in Fig. 3b, c and d (see also ESI Fig. S5†). The relative change of the PBE (w/o SOC) bandgaps of bulk materials and the corresponding MP2 HOMO–LUMO gaps of clusters *versus* x from 0 to 4 agree quite well. With the I atom gradually substituted by BH_4 , the bandgap of the admixture gradually increases, as shown in Table 2. Especially when $x \leq 2$, all the bandgaps fall in the range of the visible spectrum. When $x \geq 3$, the gaps extend to the violet and ultraviolet regions. The relatively large bandgaps of the studied 2D hybrid perovskites are not suitable for visible light absorption, which makes them less attractive as solar cell materials. However, for application in other optoelectronic devices, such as LED, the color of emitted light is also important. For this reason, 2D hybrid perovskites may be useful. For the experimentally synthesized 2D hybrid perovskites, such as $BA_2PbI_2Br_2$ and BA_2PbBr_4 , the light emission is from blue to purple, corresponding to bandgaps in the range of 2.5–3.2 eV.⁴ For the studied 2D hybrid perovskites with BH_4 , most of the estimated bandgaps based on the experimental values of BA_2PbI_4 , BA_2SnI_4 and BA_2GeI_4 fall in the range of 2.0–3.2 eV, as shown in Table 2. Also, these 2D hybrid perovskites may be applied as photoluminescent materials, where the excitation source is usually invisible light, such as ultraviolet.

In the Wannier model, the exciton binding energy is inversely proportional to the square of the dielectric constant of the material, which becomes smaller for larger bandgaps due to lower screening upon excitation. Therefore, it is possible to establish an empirical relationship between the exciton binding energy and the bandgap of semiconductors with direct bandgaps. In 3D organic–inorganic hybrid perovskites, we have been able to establish such a relationship by fitting to the available experimental data. The exciton binding energies estimated from the empirical relationship for the 3D hybrid perovskites agree well with the experimental data.³⁵ Here, by fitting to the data of the exciton binding energy and the fundamental gap of the studied clusters and a number of 2D hybrid perovskites^{42,44,45} (see Table S3†), we obtain the following relationship between the fundamental gap (E_g) and the exciton binding energy (E_b):³⁵

$$\log_{10}[E_b(\text{meV})] = 3.8824 - 3.9706 \times \exp[-0.3673 \times E_g(\text{eV})]. \quad (1)$$

As shown in ESI Fig. S6† the quality of the fit is excellent, suggesting that eqn (1) can provide a good description of the relationship between the exciton binding energy and bandgap. The exciton binding energy in the cluster model is calculated as the difference between the HOMO–LUMO and optical gaps.

Table 2 Bandgaps (eV) of the bulk admixtures $BA_2MI_{4-x}(BH_4)_x$ ($M = Pb, Sn, Ge; x = 1-4$) derived from the experimental value^{34,42,43} when $x = 0$ by using the relative gap increment from the cluster model and the PBE + SOC results. These relative gap changes are shown in Fig. 3. The gap of BA_2PbI_4 that we used for the calculations is 2.24 eV. In each case, the value in parentheses is the exciton binding energy (in meV) calculated using eqn (1)

M	$x = 0$	1		2		3		4	
	Exp.	MP2	PBE + SOC	MP2	PBE + SOC	MP2	PBE + SOC	MP2	PBE + SOC
Pb	2.24 ^a /2.88 ^b	2.48 (193)	2.55 (212)	2.89 (323)	2.79 (287)	3.44 (576)	3.34 (522)	4.44 (1273)	3.78 (780)
Sn	1.98 ^c	2.25 (140)	2.16 (122)	2.69 (254)	2.70 (257)	3.27 (487)	3.56 (643)	4.03 (952)	3.76 (767)
Ge	1.80 ^c	2.14 (118)	1.82 (70)	2.80 (290)	2.85 (308)	3.70 (728)	3.20 (454)	3.94 (888)	3.22 (463)

^a Experimental value in ref. 34. ^b Experimental value in ref. 42. ^c Experimental value in ref. 43.

The bandgap of $\text{BA}_2\text{Pb}(\text{BH}_4)_4$ is the sum of the experimental gap of BA_2PbI_4 (2.24 eV) and the gap change (1.54 eV) calculated using the PBE + SOC results in Fig. 3b. With the empirical relationship eqn (1), we can use the predicted bandgaps of the $\text{BA}_2\text{M}(\text{BH}_4)_4$ to estimate the exciton binding energy of these materials. The results are shown in Table 2, and are 780, 767 and 463 meV for $\text{M} = \text{Pb}, \text{Sn}, \text{Ge}$, respectively. The highest exciton binding energy is comparable to the 900 meV value of monolayer black phosphorus reported recently.⁴⁶ So we come to the conclusion that the bandgap and the exciton binding energies of hybrid perovskites can not only be increased by reducing the dimensionality but also by replacing halogens (e.g. I) with superhalogen moieties (e.g. BH_4), thus extending the functionality of hybrid perovskites beyond solar energy conversion.

Conclusions

In summary, a systematic theoretical study of 2D $\text{BA}_2\text{MI}_{4-x}(\text{BH}_4)_x$ ($\text{M} = \text{Ge}, \text{Sn}, \text{Pb}; x = 0-4$) hybrid perovskites shows that replacement of halogens with superhalogens can increase the bandgap and exciton binding energies much, as seen from the lowering of dimensionality. Thus, quantum confinement can be combined with compositional change of BA_2MI_4 hybrid perovskites to create materials with improved optoelectronic properties. In particular, the exciton binding energy of $\text{BA}_2\text{Pb}(\text{BH}_4)_4$ is close to that of monolayer black phosphorus. The potential of these hybrid perovskites for optoelectronic and photoluminescent applications, in addition to efficient photovoltaic devices, makes these materials a fertile ground for physicists, chemists, and material scientists.

Acknowledgements

This work was supported in part by the U.S. Department of Energy, Office of Basic Energy Sciences, Division of Materials Sciences and Engineering under Award DE-FG02-96ER45579, by the NSFC (21203096, 11374160, 51522206, 11574151), by the NSF of Jiangsu Province (BK20130031), by PAPD, by the Fundamental Research Funds for the Central Universities (no. 30915011203), and by the New Century Excellent Talents in University (NCET-12-0628). Resources of the National Energy Research Scientific Computing Center supported by the Office of Science of the U.S. Department of Energy under Contract DE-AC02-05CH11231 are acknowledged. This material is also based upon work performed using computational resources supported by the University of Tennessee and Oak Ridge National Laboratory's Joint Institute for Computational Sciences (<http://www.jics.utk.edu>). Any opinions, findings, and conclusions or recommendations expressed in this material are those of the author(s) and do not necessarily reflect the views of the University of Tennessee, Oak Ridge National Laboratory, or the Joint Institute for Computational Sciences.⁴⁷ QY acknowledges the China Scholarship Council for sponsoring his visit to Virginia Commonwealth University

where this work was conducted. We also acknowledge the support from the Shanghai Supercomputer Center.

References

- 1 A. Kojima, K. Teshima, Y. Shirai and T. Miyasaka, *J. Am. Chem. Soc.*, 2009, **131**, 6050–6051.
- 2 D. B. Mitzi, Synthesis, Structure, and Properties of Organic-Inorganic Perovskites and Related Materials, in *Progress in Inorganic Chemistry*, John Wiley & Sons, Inc., 2007, pp. 1–121.
- 3 G. C. Papavassiliou, *Prog. Solid State Chem.*, 1997, **25**, 125–270.
- 4 L. Dou, A. B. Wong, Y. Yu, M. Lai, N. Kornienko, S. W. Eaton, A. Fu, C. G. Bischak, J. Ma, T. Ding, N. S. Ginsberg, L.-W. Wang, A. P. Alivisatos and P. Yang, *Science*, 2015, **349**, 1518–1521.
- 5 G. Lanty, K. Jemli, Y. Wei, J. Leymarie, J. Even, J.-S. Lauret and E. Deleporte, *J. Phys. Chem. Lett.*, 2014, **5**, 3958–3963.
- 6 Y. Takeoka, K. Asai, M. Rikukawa and K. Sanui, *Bull. Chem. Soc. Jpn.*, 2006, **79**, 1607–1613.
- 7 D. B. Mitzi, *J. Chem. Soc., Dalton Trans.*, 2001, 1–12.
- 8 T. Baikie, Y. Fang, J. M. Kadro, M. Schreyer, F. Wei, S. G. Mhaisalkar, M. Graetzel and T. J. White, *J. Mater. Chem. A*, 2013, **1**, 5628–5641.
- 9 M. Saba, F. Quochi, A. Mura and G. Bongiovanni, *Acc. Chem. Res.*, 2016, **49**, 166–173.
- 10 V. D'Innocenzo, G. Grancini, M. J. P. Alcocer, A. R. S. Kandada, S. D. Stranks, M. M. Lee, G. Lanzani, H. J. Snaith and A. Petrozza, *Nat. Commun.*, 2014, **5**.
- 11 S. D. Stranks, G. E. Eperon, G. Grancini, C. Menelaou, M. J. Alcocer, T. Leijtens, L. M. Herz, A. Petrozza and H. J. Snaith, *Science*, 2013, **342**, 341–344.
- 12 H. Zhou, Q. Chen, G. Li, S. Luo, T.-B. Song, H.-S. Duan, Z. Hong, J. You, Y. Liu and Y. Yang, *Science*, 2014, **345**, 542–546.
- 13 N.-G. Park, *J. Phys. Chem. Lett.*, 2013, **4**, 2423–2429.
- 14 G. Xing, N. Mathews, S. S. Lim, N. Yantara, X. Liu, D. Sabba, M. Grätzel, S. Mhaisalkar and T. C. Sum, *Nat. Mater.*, 2014, **13**, 476–480.
- 15 X. Y. Chin, D. Cortecchia, J. Yin, A. Bruno and C. Soci, *Nat. Commun.*, 2015, **6**.
- 16 F. Deschler, M. Price, S. Pathak, L. E. Klintberg, D.-D. Jarausch, R. Högler, S. Hüttner, T. Leijtens, S. D. Stranks, H. J. Snaith, M. Atatüre, R. T. Phillips and R. H. Friend, *J. Phys. Chem. Lett.*, 2014, **5**, 1421–1426.
- 17 J. Song, J. Li, X. Li, L. Xu, Y. Dong and H. Zeng, *Adv. Mater.*, 2015, **27**, 7162–7167.
- 18 J. Song, L. Xu, J. Li, J. Xue, Y. Dong, X. Li and H. Zeng, *Adv. Mater.*, 2016, **28**, 4861–4869.
- 19 G. L. Gutsev and A. I. Boldyrev, *Chem. Phys.*, 1981, **56**, 277–283.
- 20 P. Schouwink, M. B. Ley, A. Tissot, H. Hagemann, T. R. Jensen, L. Smrčok and R. Černý, *Nat. Commun.*, 2014, **5**, 5706.

- 21 H. Fang and P. Jena, *J. Mater. Chem. A*, 2016, **4**, 4728–4737.
- 22 J. P. Perdew, K. Burke and M. Ernzerhof, *Phys. Rev. Lett.*, 1996, **77**, 3865–3868.
- 23 G. Kresse and J. Furthmüller, *Phys. Rev. B: Condens. Matter*, 1996, **54**, 11169–11186.
- 24 S. Grimme, *J. Comput. Chem.*, 2006, **27**, 1787–1799.
- 25 H. Fang, M. T. Dove and K. Refson, *Phys. Rev. B: Condens. Matter*, 2014, **90**, 054302.
- 26 H. J. Monkhorst and J. D. Pack, *Phys. Rev. B: Solid State*, 1976, **13**, 5188–5192.
- 27 A. Fonari and C. Sutton, *Effective Mass Calculator*, 2012.
- 28 M. J. Frisch, G. W. Trucks, H. B. Schlegel, G. E. Scuseria, M. A. Robb, J. R. Cheeseman, J. J. A. Montgomery, T. Vreven, K. N. Kudin, J. C. Burant, J. M. Millam, S. S. Iyengar, J. Tomasi, V. Barone, B. Mennucci, M. Cossi, G. Scalmani, N. Rega, G. A. Petersson, H. Nakatsuji, M. Hada, M. Ehara, K. Toyota, R. Fukuda, J. Hasegawa, M. Ishida, T. H. Y. Nakajima, O. Kitao, H. Nakai, M. Klene, X. Li, J. E. Knox, H. P. Hratchian, J. B. Cross, V. Bakken, C. Adamo, J. Jaramillo, R. Gomperts, R. E. Stratmann, O. Yazyev, A. J. Austin, R. Cammi, C. Pomelli, J. W. Ochterski, P. Y. Ayala, K. Morokuma, G. A. Voth, P. Salvador, J. J. Dannenberg, V. G. Zakrzewski, S. Dapprich, A. D. Daniels, M. C. Strain, O. Farkas, D. K. Malick, A. D. Rabuck, K. Raghavachari, J. B. Foresman, J. V. Ortiz, Q. Cui, A. G. Baboul, S. Clifford, J. Cioslowski, B. B. Stefanov, G. Liu, A. Liashenko, P. Piskorz, I. Komaromi, R. L. Martin, D. J. Fox, T. Keith, M. A. Al-Laham, C. Y. Peng, A. Nanayakkara, M. Challacombe, P. M. W. Gill, B. Johnson, W. Chen, M. W. Wong, C. Gonzalez and J. A. Pople, Gaussian, Inc., Wallingford, CT, 2004.
- 29 C. Møller and M. S. Plesset, *Phys. Rev.*, 1934, **46**, 618–622.
- 30 E. Runge and E. K. U. Gross, *Phys. Rev. Lett.*, 1984, **52**, 997–1000.
- 31 C. Lee, W. Yang and R. G. Parr, *Phys. Rev. B: Condens. Matter*, 1988, **37**, 785–789.
- 32 A. D. Becke, *Phys. Rev. A*, 1988, **38**, 3098–3100.
- 33 P. Umari, E. Mosconi and F. De Angelis, *Sci. Rep.*, 2014, **4**, 4467.
- 34 D. H. Cao, C. C. Stoumpos, O. K. Farha, J. T. Hupp and M. G. Kanatzidis, *J. Am. Chem. Soc.*, 2015, **137**, 7843–7850.
- 35 H. Fang and P. Jena, *J. Phys. Chem. Lett.*, 2016, **7**, 1596–1603.
- 36 L.-Y. Huang and W. R. L. Lambrecht, *Phys. Rev. B: Condens. Matter*, 2013, **88**, 165203.
- 37 J. H. Noh, S. H. Im, J. H. Heo, T. N. Mandal and S. I. Seok, *Nano Lett.*, 2013, **13**, 1764–1769.
- 38 C. Katan, L. Pedesseau, M. Kepenekian, A. Rolland and J. Even, *J. Mater. Chem. A*, 2015, **3**, 9232–9240.
- 39 F. Chiarella, A. Zappettini, F. Licci, I. Borriello, G. Cantele, D. Ninno, A. Cassinese and R. Vaglio, *Phys. Rev. B: Condens. Matter*, 2008, **77**, 045129.
- 40 N. Kitazawa, Y. Watanabe and Y. Nakamura, *J. Mater. Sci.*, 2002, **37**, 3585–3587.
- 41 G. E. Eperon, S. D. Stranks, C. Menelaou, M. B. Johnston, L. M. Herz and H. J. Snaith, *Energy Environ. Sci.*, 2014, **7**, 982–988.
- 42 T. Ishihara, J. Takahashi and T. Goto, *Phys. Rev. B: Condens. Matter*, 1990, **42**, 11099–11107.
- 43 D. B. Mitzi, *Chem. Mater.*, 1996, **8**, 791–800.
- 44 D. S. Hamilton, R. S. Meltzer, M. D. Sturge and T. Ishihara, *J. Lumin.*, 1994, **60**, 269–274.
- 45 X. Hong, T. Ishihara and A. V. Nurmikko, *Phys. Rev. B: Condens. Matter*, 1992, **45**, 6961–6964.
- 46 X. Wang, A. M. Jones, K. L. Seyler, V. Tran, Y. Jia, H. Zhao, H. Wang, L. Yang, X. Xu and F. Xia, *Nat. Nanotechnol.*, 2015, **10**, 517–521.
- 47 M. R. Fahey, R. Budiardja, L. Crosby and S. McNally, Deploying Darter – A Cray XC30 System, in *Supercomputing: 29th International Conference, ISC 2014, Leipzig, Germany, June 22–26, 2014. Proceedings*, ed. J. M. Kunkel, T. Ludwig and H. W. Meuer, Springer International Publishing, Cham, 2014, pp. 430–439.